



Statistical calibration of ultrasonic fatigue testing machine and probabilistic fatigue life estimation

Sina Safari ^a,*, Diogo Montalvão ^b, Pedro R. da Costa ^{c,d}, Luís Reis ^d, Manuel Freitas ^{c,d}

^a Department of Mechanical Engineering, University of Bristol, Bristol, BS8 1TR, UK

^b ADDISONIC Research Cluster, Department of Design and Engineering, Faculty of Science and Technology, Bournemouth University, Poole House, Talbot Campus, Poole, BH12 5BB, UK

^c Atlântica, Instituto Universitário, Fábrica de Pólvora de Barcarena, 2730-036, Barcarena, Portugal

^d IDMEC, Instituto Superior Técnico, Universidade de Lisboa, Av. Rovisco Pais, 1, 1050-099, Lisboa, Portugal

ARTICLE INFO

MSC:
00-01
99-00

Keywords:

Ultrasonic fatigue testing
Calibration
Hierarchical Bayesian method
Cyclic lifetime
Uncertainty quantification (UQ)

ABSTRACT

A new statistical technique is proposed to quantify the experimental uncertainty observed during ultrasonic fatigue testing of metals and its propagation into the stress-lifetime predictive curve. Hierarchical Bayesian method is employed during the calibration and operation steps of ultrasonic fatigue testing for the first time in this paper. This is particularly important due to the significant dispersion observed in stress-life data within the high and very high cycle fatigue regimes. First, the measurement systems, including displacement laser readings and high-speed camera system outputs, are cross-calibrated. Second, a statistical learning approach is applied to establish the stress-deformation relationship, leveraging Digital Image Correlation (DIC) measurements of strain and laser displacement measurements at the ultrasonic machine specimen's tip. Third, an additional hierarchical layer is introduced to infer the uncertainty in stress-life curves by incorporating learned stress distributions and the distribution of fatigue failure cycles. The results identify key sources of uncertainty in UFT and demonstrate that a hierarchical Bayesian approach provides a systematic framework for quantifying these uncertainties.

1. Introduction

Understanding fatigue is crucial for structural design, monitoring, and durability analysis. With modern engineering structures, such as aerospace structures and power plant components, required to sustain extremely long lifespans, research efforts have increasingly focused on high-cycle fatigue and Very High-Cycle Fatigue (VHCF) [1]. VHCF typically refers to fatigue scenarios where the component's lifespan exceeds 10^7 cycles and initially were called GigaCycle Fatigue [2,3]. A historical review of VHCF can be found in [4]. Fatigue testing up to the VHCF regime is time-consuming using conventional fatigue testing machines with an operating frequency of 10–400 Hz. In 1951, Mason [5] pioneered the development of the Ultrasonic Fatigue Testing (UFT) machine, which operates on resonance theory at a frequency of 20 kHz. This innovation significantly reduced the duration of fatigue testing in the VHCF regime from months to days [3,6].

Over the past 10 to 20 years, there have been a considerable number of publications, the construction of new UFT machines, the introduction of innovative experimental methodologies, and the broadening of capabilities to encompass a diverse range of materials and stress

profiles [7]. Tridello et al. [8] provided an overview of the VHCF testing and challenges, including testing procedures, failure mechanisms, microstructural and specimen size effects, temperature effects and statistical modelling. These factors all influence the accuracy of fatigue life prediction using VHCF. The nature and mechanism of failure under VHCF [4] and its frequency-dependency [9] in metals are being investigated by the scientific community. However, the uncertainty associated with the testing procedure, applied load, and measurement devices during ultrasonic fatigue tests is generally neglected, especially when new measurement systems are used.

Testing procedure starts with machine calibration that is finding a relationship between strain in the high stress region of the test specimen and tip displacement of the specimen in the uniaxial case [10]. The accuracy of stress-life data as the outcome of UFT depends on the accuracy of the produced relationship during machine calibration. In fact, part of the variability observed in UFT testing is due to variability arising from machine operation, measurement systems, and the specimen material itself. This variability could be statistically quantified if the calibration relationship is established using multiple recordings

* Corresponding author.

E-mail address: sina.safari@bristol.ac.uk (S. Safari).

on a batch of specimens for a specific material. This paper presents a statistical technique to systematically quantify the uncertainties that arise specifically during calibration and enables their propagation in the stress-life curve produced using the UFT.

The calibration process for the UFT machines has been briefly outlined in the Japan Welding Engineering Society WES 1112:2017 [10]. This process mainly provides recommendations for stress level control and temperature control. In principle, two types of loading conditions were considered in this standard, namely axial and torsional loading. However, other types of loading conditions are allowed, provided there is an appropriate finite element analysis [11]. For axial specimens, an accurate and inexpensive way to determine stress levels is to find out the relationship between stress amplitude and tip displacement of the test specimen. This relationship is commonly derived by measuring the displacement at the tip and the maximum strain at the higher stress region of the test specimen. An alternative method is using analytical equations [12]. In this paper, a displacement laser is used to measure tip displacements, and a DIC system is used to measure strains. This method enables one to study uncertainties involved in measurement systems and processes based on experimental data without any pre-assumptions.

To deal with the uncertainties, probabilistic approaches gained interest recently, especially to characterise fatigue lifetime (S-N) curves for uniaxial [13] and multiaxial [14] fatigue experimental data. The resulting stress-life curves are considered probabilistic S-N (P-S-N) curves. The Hierarchical Bayesian (HB) method [15] is used in this work to handle the uncertainties and produce models capable of propagating those uncertainties into the S-N curves. The advantage of the HB method is that it works out uncertainties not only within a single data set but also across multiple data sets and enables the information learned at higher levels of the calculation workflow to influence parameter estimates at lower levels, making the model robust.

Although microstructure variability plays a key role and may drive the large amount of uncertainty involved in the UFT, one may see uncertainty through the lens of a system with input and output. In this case, an ensemble of datasets will represent the variability in the system. For example, the ultimate product of a UFT machine is the stress (strain)-life curves. The variability in life (here, the number of cycles) can be estimated by breaking a representative number of specimens for a specific stress level. Besides, the uncertainty in the stress (strain) level can be estimated through the measured strain by repeating the measurement multiple times. This way, one may not only capture the uncertainty due to material variability but also the testing equipment.

In this work, a Digital Image Correlation (DIC) system is used to measure displacement and strain under cyclic loading and a laser system is used to measure the specimen's tip displacement. The uncertainty sourced from the measurement system and UFT machine operation is reflected on the calibration curve and subsequently on the stress-life curves. The rest of this paper is structured as follows: Section 2 introduces the UFT machine and its components; Section 3 presents a probabilistic framework for the calibration of UFT machine and the fatigue lifetime curves in the VHCF regime; in Section 4 experimental calibration is demonstrated; Section 5 shows the stress-life models for the VHCF regime; and finally, Section 7 offers the conclusions drawn from this study.

2. Ultrasonic fatigue testing machine

Ultrasonic fatigue testing differs from conventional fatigue testing by using forced vibration at the specimen's fundamental frequency, while conventional tests use a frequency far below the fundamental. In general, UFT systems are composed of four main parts: a resonance system (piezoelectric transducer, a booster, a horn, and finally the specimen), a measurement system (displacement measurement laser, pyrometer, DIC system, or strain gauges), a cooling system (i.e., a

compressor and its spraying nozzle), a power and a data acquisition system with a control software. The UFT system requires careful design of the testing machine and specimens so that their working frequencies match. The working mechanism of UFT machines has been well documented [16]. In this work, the UFT system is designed and built in-house within the ADDISONIC Research Cluster (ARC) at Bournemouth University. Fig. 1a shows different components of the system. Fig. 1b shows the control software including real-time block signal of measured tip displacement, block average of the input power, the block average of the displacement amplitude, and the main frequency of the block signal.

The working frequency of the machine is between 19.45 and 20.45 kHz. A piezoelectric transducer excites the assembled components axially, and the booster and horn amplify the displacement using the resonance theory and an axial mode shape. Since the specimen cycles with a very high frequency, the temperature of the specimen should be controlled, which is done using a pyrometer (i.e., thermometer) and a cooling system spraying cold air in the high-stress volume of the specimen (i.e., control volume). That is the middle of the specimen for an hourglass shape. The temperature is controlled between the room temperature of 21 °C and a higher threshold of 30 °C as recommended by the Japanese standard [17].

This work uses tip displacement measurement for controlling the level of stress in the location of the control volume of the specimen via building a relationship between tip displacement and strain amplitude [17]. The measurement system uses a laser at the tip of the specimen to monitor displacement in real-time and provides feedback to control the excitation power. In this work, Keyence LK-H027 Ultra High-Speed/High-Accuracy laser displacement sensor head with 0.02 μm repeatability is used, and the laser measurement sampling frequency is 200 kHz. A simple linear controller is used. A simple linear controller is used to calculate the maximum absolute value of the main harmonics of the current tip displacement and adjust the excitation power proportionally to the ratio between the target and measured displacement. The tolerance assumed here is 10⁻⁴. It should be noted that saturation thresholds for maximum operational power are implemented to ensure safe operation.

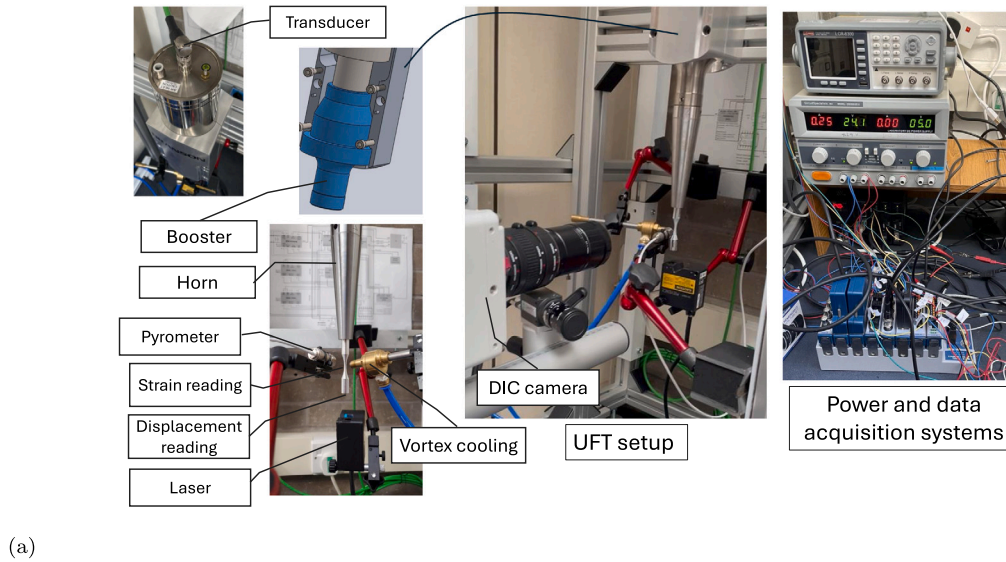
A DIC system with a Q-450 high-speed camera up to a sampling frequency of 125 kHz from Dantec Dynamics is used to measure the strain in the location of the control volume on the specimen. The resolution is typically around 1 μm and 0.01% strain. Istra4D DIC application [18] is used for data collection and correlation analysis. A cross-validation between laser and DIC measurements is carried out in Section 4.1 to prove the accuracy of measurements. This is a non-contact measurement technique that differs from other methods, such as using strain gauges [19]. It is noteworthy that the specimens are sprayed with white paint and black speckles on one side for DIC measurement and completely black on the other side to improve the accuracy in temperature measurement using the pyrometer.

After the initial calibration of the machine and discovering the relationship between tip displacement and the stress in the control volume of the specimen, UFT starts by intermittently vibrating the specimen up to a specific tip displacement level until it fails. In each vibrating phase, the temperature rises to the threshold, where the vibration stops, and after cooling for a couple of seconds, the vibration continues. The failure is picked up with a dramatic change in the working frequency so that the machine stops operating, or the specimen breaks. The whole process is controlled by the control software in Fig. 1b.

3. Hierarchical Bayesian (HB) method

In the Bayesian approach, the uncertainty in model parameters is represented by a probability density function (PDF) and is determined using Bayes' theorem as follows:

$$p(\theta|\mathcal{D}) = \frac{p(\mathcal{D}|\theta)p(\theta)}{p(\mathcal{D})} \quad (1)$$



(a)



(b)

Fig. 1. Ultrasonic fatigue testing system at the ADDISONIC Research Cluster (a) experimental setup and (b) control software setup.

where $p(\theta|\mathcal{D})$ is the posterior probability distribution function of the mathematical model $M(\theta) \in \mathcal{M}$ parametrised by variable $\theta \in \mathbb{R}^{N_\theta}$. In the Bayesian approach, the posterior probability is calculated to update our belief about a parameter or hypothesis after incorporating new evidence or data. It represents the revised probability of a model or parameter given the observed data. Here, \mathcal{M} is a set of models or a single model with probabilistic parameter values that describe the functional relationship between input and output data collected from multiple measurements, and N_θ is the number of unknown parameters. For example, the unknown parameters are the parameters of a linear model between specimen tip displacement and strain in the control volume, as well as the parameters of the stress-life model. In Eq. (1), $p(\mathcal{D}|\theta)$ is the likelihood, which expresses the probability of observing

experimental data \mathcal{D} given the parameter value θ . From a minimisation problem perspective, the likelihood function enables minimising the error between model estimation Y and observed data \hat{Y} . The existing belief or knowledge about the parameters is defined by prior distribution $p(\theta)$ and $p(\mathcal{D})$ is the probability of observing the data \mathcal{D} in the experiments. In the Bayes theorem, $p(\mathcal{D})$ is also called evidence or marginal likelihood, which represents the total probability of observing the data \mathcal{D} , considering all possible values of parameters θ . The evidence is often neglected as it acts as a normalisation constant [20] in Bayesian parameter estimation, where relative probabilities are more important than absolute values. The model may be expressed as:

$$Y_i = M(\theta) + \varepsilon_i \quad (2)$$

where Y_i is the model output, and $\varepsilon_i \in \mathbb{R}$ is the prediction error, which is characterised by an additive zero-mean Gaussian White Noise (GWN) with variance $\sigma^2 \in \mathbb{R}$. By extending the parameter set to include σ , one can estimate its value as well during the model parameter updating process, or so-called training.

In the context of the classical Bayesian method, the posterior probability distribution function of the updated parameter θ_i and the prediction error parameter σ_i can be expressed for a single dataset \mathcal{D}_i according to the rule of product in probability:

$$p(\theta_i, \sigma_i | \mathcal{D}_i) \propto p(\mathcal{D}_i | \theta_i, \sigma_i) p(\theta_i) p(\sigma_i) \quad (3)$$

The classical Bayesian method for estimating parameter uncertainty fails to fully capture the overall variability. As the number of datasets increases, the uncertainty decreases, a phenomenon often referred to as “noise mitigation” [21]. To deal with this shortfall, the HB method incorporates the dependency and variability of the model parameters across different datasets [22]. In this work, the unknown parameters θ are modelled by normal distribution as:

$$p(\theta) = \mathcal{N}(\mu_\theta, \Sigma_{\theta\theta}) \quad (4)$$

where $\mu_\theta \in \mathbb{R}^{N_\theta}$ is the mean value of the unknown parameters, and $\Sigma_{\theta\theta} \in \mathbb{R}^{N_\theta \times N_\theta}$ is the covariance matrix. The mean and covariance parameters are the new set of parameters that are often called hyperparameters. The unknown parameters corresponding to the dataset i are free to vary across total datasets, which are considered independent samples. Eq. (3) can be modified for the HB method to calculate the posterior distribution of the hyperparameters as follows:

$$p(\{\theta_i\}_{i=1}^n, \mu_\theta, \Sigma_{\theta\theta}, \sigma | \mathcal{D}) \propto p(\{\mathcal{D}_i\}_{i=1}^n | \{\theta_i\}_{i=1}^n, \mu_\theta, \Sigma_{\theta\theta}, \sigma) \times p(\{\theta_i\}_{i=1}^n, \mu_\theta, \Sigma_{\theta\theta}, \sigma) \quad (5)$$

where $p(\mu_\theta, \Sigma_{\theta\theta})$ is the prior distribution of hyperparameters and $p(\mathcal{D} | \mu_\theta, \Sigma_{\theta\theta})$ is the likelihood function of all datasets \mathcal{D} . The hierarchy of models emerges in Eq. (5) where the parameters of the main model θ are conditional on the estimated parameters of another model, which is the normal distribution model according to Eq. (4). In the case of considering N_D independent datasets, the likelihood function $p(\mathcal{D} | \mu_\theta, \Sigma_{\theta\theta})$ can be expressed as:

$$p(\{\mathcal{D}_i\}_{i=1}^n | \{\theta_i\}_{i=1}^n, \mu_\theta, \Sigma_{\theta\theta}, \sigma) = \prod_{i=1}^n p(\mathcal{D}_i | M(\theta_i), \sigma). \quad (6)$$

Based on the diagram shown in Fig. 2, the joint prior distribution is characterised as the multiplication of distributions, given as:

$$p(\{\theta_i\}_{i=1}^n, \mu_\theta, \Sigma_{\theta\theta}, \sigma) \propto p(\mu_\theta, \Sigma_{\theta\theta}) p(\sigma) \prod_{i=1}^n \mathcal{N}(\theta_i | \mu_\theta, \Sigma_{\theta\theta}). \quad (7)$$

It should be noted that the prior distribution for the standard deviation σ is a half-normal distribution. The full posterior distribution in Eq. (5) can now be expressed as

$$p(\{\theta_i\}_{i=1}^n, \mu_\theta, \Sigma_{\theta\theta}, \sigma | \mathcal{D}) \propto p(\mu_\theta, \Sigma_{\theta\theta}) p(\sigma) \prod_{i=1}^n \mathcal{N}(\mathcal{D}_i | M(\theta_i), \sigma) \times \mathcal{N}(\theta_i | \mu_\theta, \Sigma_{\theta\theta}) \quad (8)$$

The above equation and the principle from Fig. 2b show that the hyperparameters $\mu_\theta, \Sigma_{\theta\theta}, \sigma$ could be inferred from the posterior distribution. To achieve this, the joint probability distribution in Eq. (8) must be marginalised over the parameter space. The marginalisation or parameter estimation is carried out by Markov Chain Monte Carlo (MCMC) sampling methods. Typical MCMC sampling methods include random walk Metropolis–Hastings [23] or Gibbs sampling [24]. In this work, the Hamiltonian Monte Carlo (HMC) method with the No-U-Turn Sampler (NUTS) algorithm [20] is used to estimate the parameters. HMC is an MCMC variant that avoids random walks in the parameter space by taking a series of steps informed by first-order gradient information. This feature allows it to converge to target distributions much quicker than other methods. However, its performance is highly sensitive to two user-specified parameters: a step size and a desired

Table 1
Chemical composition of EN8 steel.

Composition	Fe	C	Mn	Mo	P	Si	S
Percentage (wt.%)	Bal.	0.36–0.44	0.6–1.0	0.15	0.05	0.1–0.4	0.05

Table 2
Mechanical properties of EN8 steel used in this study.

Young modulus (GPa)	Yield strength (MPa)	Ultimate tensile strength (MPa)	Elongation (%)
200	460	886	16

number of steps. The NUTS algorithm uses recursive methods that eliminate the need to set those parameters, avoiding user intervention or costly tuning runs. In this work, the implementation in the PyMC package [25] is used to perform sampling for hyperparameter estimation. The above implementation is summarised in the flowchart in Fig. 2a, and an open-source code of the model implementation used in this paper is included in the code availability section for demonstration.

4. Experimental calibration

The axisymmetric hourglass specimens have been used and widely validated in many research works concerning ultrasonic fatigue testing of different materials [7]. A working specimen is designed in this study. The design of the specimen is done analytically in this work using the method presented in [12], which is used to achieve the initial geometry of the specimen. Also, this can be done via geometry optimisation with the application of the finite element method (FEM) [26]. Then, the FE model of the specimen attached to the UFT machine is developed to validate the design and tune the geometry.

The material used for the test specimen in this paper is made from cold-rolled EN8 steel with chemical composition and mechanical properties reported in Tables 1 and 2, respectively. It should be noted that the material is selected from the same batch used in [27], and mechanical properties are based on the average of tensile tests. The British standard classification of EN8 medium-strength carbon steel is BS970, most commonly known as 080M40. It is also recognised as Steel Grade 40, which is a structural material better used in engineering and construction applications. Other common names for this steel are C45 (EU), 1040 steel (USA), 45 (China), S40C (Japan), and ISO68318. Hourglass-shaped specimens for fatigue testing were machined from bars of 12.5 mm diameter. The geometry and dimensions of the specimen are shown in Fig. 3.

To address the need to calibrate the UFT machine to acquire accurate and reliable data using the equipment introduced in Section 2, the following steps are considered:

- (i) calibrate and validate the laser reading and DIC system
- (ii) make sure the intended mode shape is excited
- (iii) extract the statistical distribution of working frequency and damping of the UFT machine
- (iv) build a statistical relationship between strain measured by the DIC technique and tip displacement from laser reading data

The first two steps focus on validating the intended operational condition of the UFT machine, and the following two steps are used to generate data to calibrate the numerical models and reflect the experimental uncertainty on the stress life (S-N) predictive curve.

4.1. Measurement system and UFTM machine uncertainties

Firstly, the measurement systems, including lasers and DIC systems, are set up and their sensitivity is adjusted using standard approaches recommended by the system producers mentioned in Section 2. Afterwards, step (i) is carried out by measuring the tip displacement of the

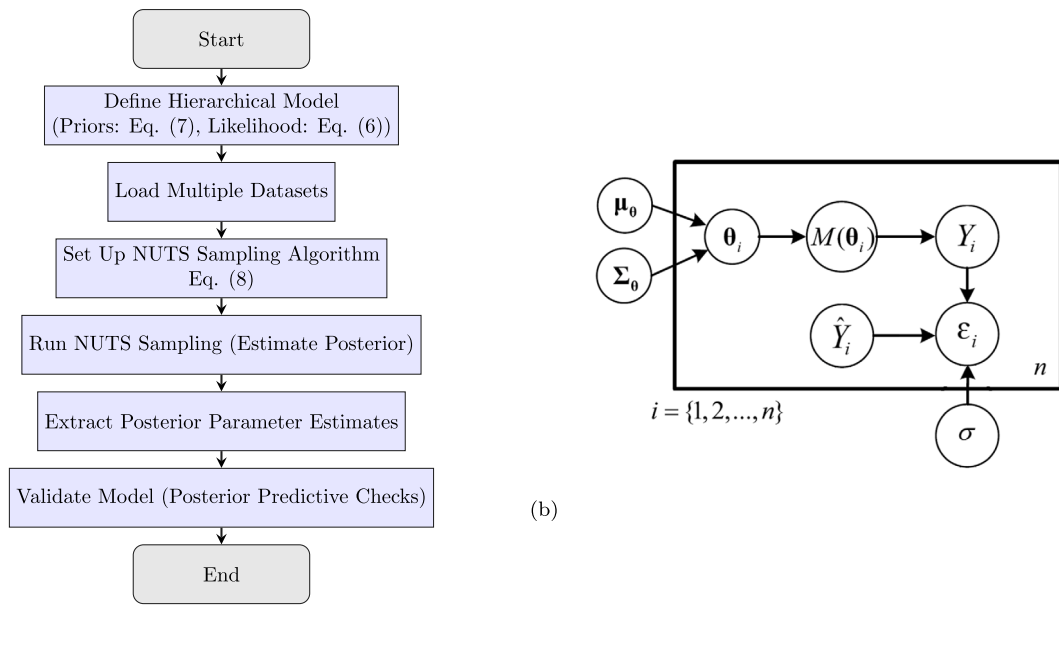


Fig. 2. Hierarchical Bayesian method (a) flowchart describing the procedure of model implementation (b) diagram of the model variable and data flow. Source: Modified and reproduced from [14].

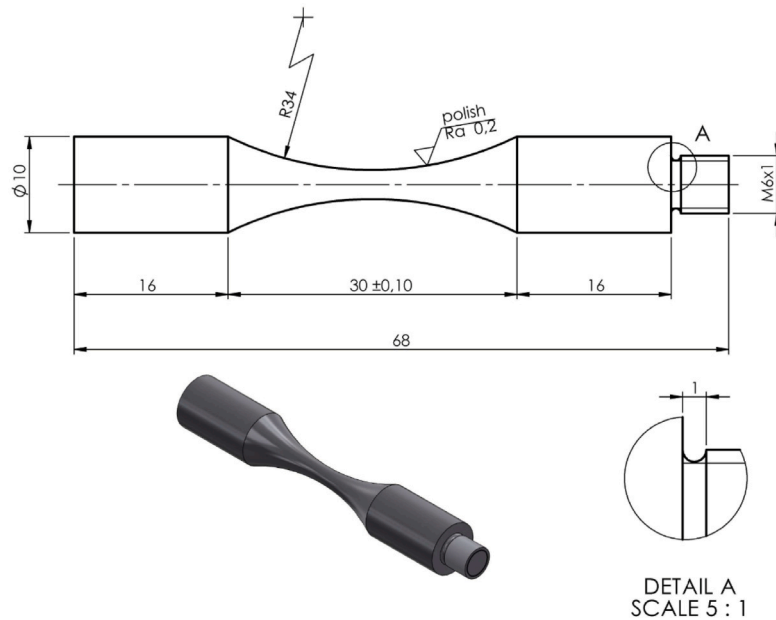


Fig. 3. Geometry and dimensions of the hourglass-shaped specimen for ultrasonic fatigue testing.

specimen using both laser and DIC systems for cross-validation between the measurements of both systems. For this purpose, the laser is set up at the bottom of the specimen (Fig. 1) and DIC is positioned in two different regions on the specimen to measure the displacement at the free end of the specimen and the end of the specimen connected to the UFT machine. The target displacement is set at $10 \mu\text{m}$ for demonstration purposes, as it is the lowest tip displacement that the measurement system may observe during the operation in this work. Therefore, a low signal-to-noise ratio (SNR) is expected for this measurement level. The calculated SNR value is 22 for the signal in Fig. 4. Fig. 4a,b shows the deformation contour at the joint and free end locations (videos in the appendix). The comparison between the measured displacements by the DIC system and laser, which is shown in Fig. 4c, indicates a

good agreement. It should be noted that the displacement at the joint location is mirrored for the purpose of comparison. Some important observations can be made. Laser measurement, especially for low amplitudes, produces noisy data that is due to experimental conditions (e.g., measurement surface, light, etc.) and sensor sensitivity. The sampling frequency of the laser has been set to 200 kHz. This produces uncertainty for the feedback controller when adjusting the applied force.

As another source of uncertainty, the DIC system reports the standard deviation of the measured displacement. This standard deviation varies between $0.25\text{--}0.5 \mu\text{m}$. The DIC system process involves image acquisition, noise reduction, and defining a Region of Interest (ROI), which is divided into subsets for tracking. Correlation techniques are used to search for the best-matching subset compared to a

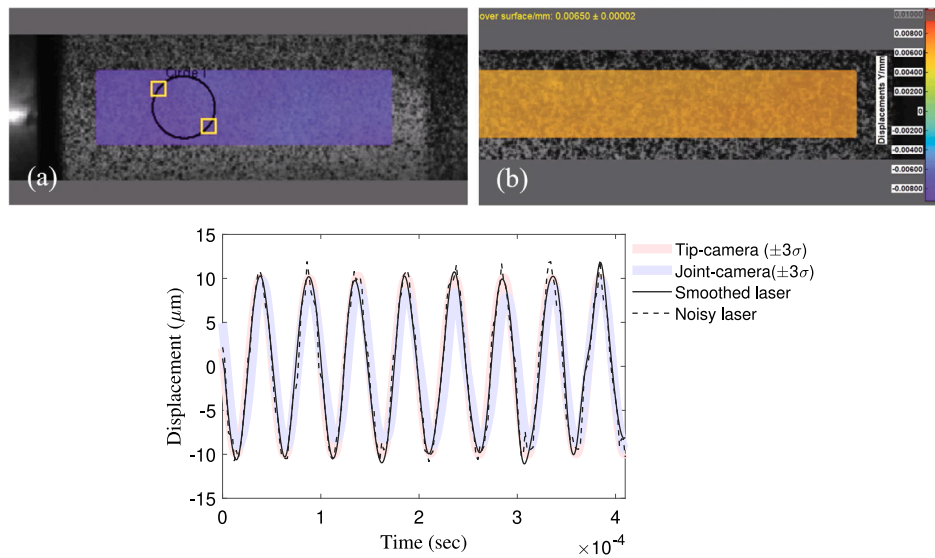


Fig. 4. Validation of laser and DIC system measurements (a) displacement contour from the DIC system at the joint location; (b) displacement contour from the DIC system at the tip location; (c) comparison of tip displacements.

reference image. This refines with sub-pixel interpolation and optimisation algorithms. Measurement accuracy is assessed through correlation residuals, which leads to the standard deviation [28]. The standard deviation calculated from correlation residuals is propagated the uncertainty arising from the high testing frequency, as it directly affects the quality of the captured images. Also, it should be noted that the circular specimen might introduce additional measurement uncertainty due to the out-of-plane motion. However, the ROI is focused on a narrow area of the specimen, and the measurement is carried out in the axial direction, averaged over the small region at the end of the specimen (see Fig. 4a). This reduces the potential error caused by the circular specimen.

Another observation is the slightly lower displacement at the joint location compared to the free end by 5%–10%, which can introduce asymmetric end deformation and eventually affect the value and location of maximum stress in the control zone in the middle of the specimen. This asymmetry is not affected by the amplitude of vibration. These kinds of slight inaccuracies are either due to the measurement system or manufacturing/assembly errors, which are inevitable as another source of uncertainty involved in UFT. Overall, the results demonstrate that the intended mode shape is excited.

With the aim of understanding the statistics of system dynamics, operational modal analysis was performed by measuring the decaying response of the tip displacement. System dynamics are characterised by the change of natural frequency and damping ratio with respect to displacement amplitude. These characteristics are reported for the entire assembly after the specimen is mounted. Therefore, variability in measured frequency for multiple runs of the experiment is expected. Also, it should be noted that damping is sourced from both material deformation and friction, mainly due to bolted joints. This can also be used later for calibrating the FE model, which is outside of the scope of this study. Fig. 5a shows the measured and filtered displacement response. The amplitude ramps up quickly when excitation starts; it continues in a steady state and decays in free vibration to zero in almost 0.2 s after excitation stops. A filter is applied to smooth the cyclic data for later analysis, preventing double zero-crossings when using the zero-crossing method. The filtered data is obtained using a third-order band-pass Butterworth filter between frequencies [20 172, 20 305] Hz. The filter characteristics are tuned to preserve only the main excited harmonic and amplitude of the signal. Fig. 5b,c shows the instantaneous frequency and damping. This means the change of frequency and damping with respect to displacement amplitude.

Higher displacement amplitude means higher stress in the middle of the specimen. The displacement amplitude used to generate the results here covers a good range of stress values experienced in the UFT of specimens in this study.

The zero-crossing method proposed in [29] is used here to extract them from the measured decay displacement response. The method measures the time period between consecutive zero-crossings and from that estimates the instantaneous frequency. Damping is estimated by analysing the amplitude decay between zero-crossings and applying the logarithmic decrement method instantaneously. It can be seen that the frequency shows slightly softening behaviour in high amplitudes, which is a typical behaviour for bolted assemblies [30]. However, the average frequency identified for the UFT machine assembly is 20 246 Hz. It can be seen from Fig. 5c that damping does not vary with amplitude, and the identified damping ratio is 0.015%. This is consistent with the results in [16] for a different UFT machine.

Since the UFT machine works at a very high frequency and the assembly consists of component joints with bolts, it is likely that the dynamic characteristics of the machine change after some test iterations. Therefore, a statistical analysis by repeating the free decay test is conducted. Fig. 6a,c presents the change of measured natural frequency and damping, respectively, over 50 test iterations. It should be noted that test parameters such as tip displacement amplitude, which results in stress in the middle section of the specimen and temperature are kept constant. It can be observed that there is over 50 Hz drop in the frequency after a couple of repetitions; however, the damping ratio varies in a specific range. This indicates the machine's working frequency is dependent on the fittings of the assembly, and that it could introduce another source of uncertainty in the measurement and fatigue life estimation. The repetition continued further, and the statistical distribution of measured frequency and damping was built as shown in Fig. 6c. The distribution shows the variation in the dynamics of the UFT machine that leads to variation of the tip-displacement and strain relationship discussed in Section 4.2. The results show sufficient consistency with the Japanese standard [10], which recommends that the cyclic frequency change should be within $\pm 0.5\%$ for test repetitions.

Overall, the results in this section indicate many sources of uncertainties throughout the test that should be systematically taken into account and carried forward in building predictive life estimation curves and eventually in life assessment analyses.

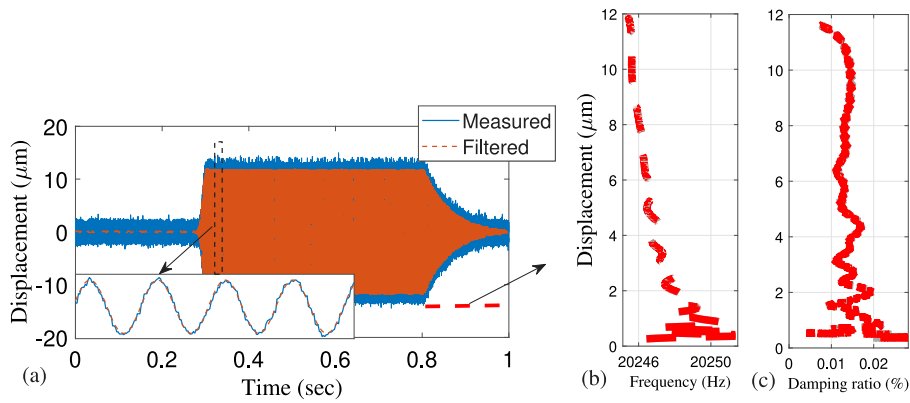


Fig. 5. Response analysis of the UFT machine for calibration (a) measured tip displacement; (b) instantaneous frequency and damping characteristics.

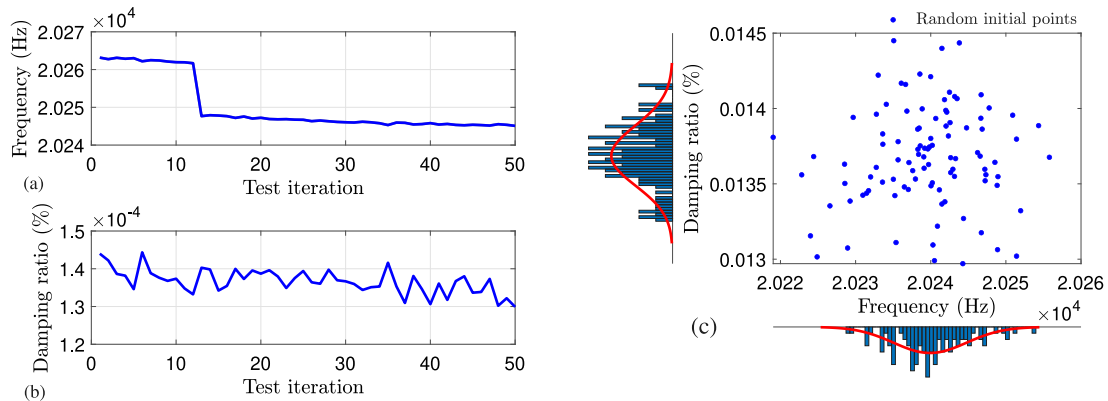


Fig. 6. Test repetition effect on dynamics of UFT machine (a) frequency trend; (b) damping trend; (c) statistical distribution of dynamic characteristics.

4.2. Probabilistic relationship of tip displacement and strain (stress)

The procedure proposed in the Japanese standard [17] to estimate the strain (or stress) level is based on a linear relationship between strain and tip displacement of the specimen. This is a particularly valid approach since the macroscale behaviour of metal specimens is well within the linear regime for the stress levels expected in the VHCF region of the stress-life curve. To achieve this, the calibration should be performed based on the results of the tip displacement amplitude and the strain at the control volume (middle of the specimen in the uniaxial hourglass types), measured either with a strain gauge or DIC system. This calibration procedure may be carried out to determine the VHCF life of any new material. It is recommended that at least five points of tip displacement amplitude should be measured within the capacity range of the testing machine [10]. However, the recommended approach does not include the uncertainties involved in the measurement system, specimen-to-specimen variation, and dynamics of the UFTM machine as discussed in Section 4.1. There are analytical techniques based on elastic calculations recommended in the standard [10] and well-developed by the authors for more complicated multiaxial loading [12]. Although these techniques are very powerful for engineering calculations, they lack probabilistic presentation.

In this section, an ensemble-based technique is proposed that uses multiple data sets to produce a statistical relationship between strain in the control volume (middle of the specimen) and tip displacement. It is shown that the statistical relationship enables one to reflect the uncertainty in the life estimation step as well. The flowchart of the proposed technique is presented in Fig. 7.

First, five different specimens are selected, and the measurement of strain (DIC) and tip displacement (laser) is repeated over 50 times. This is to include material, measurement system, and UFT machine

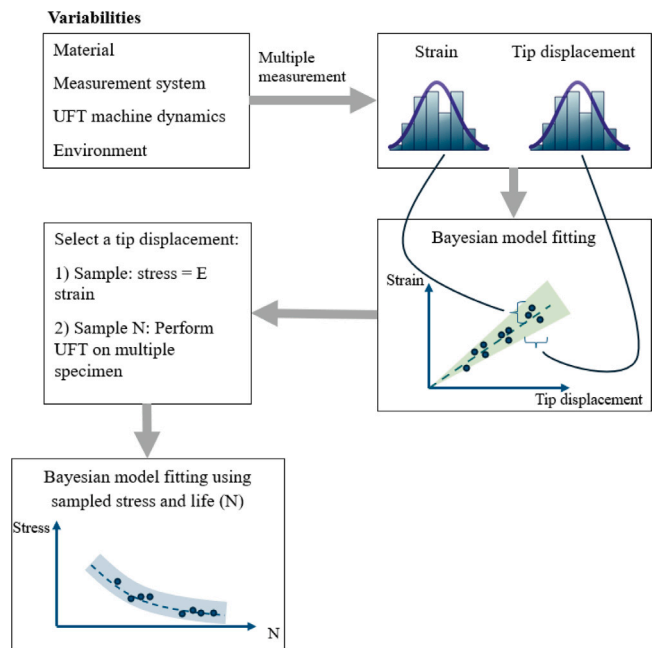


Fig. 7. Flowchart of the proposed method for a probabilistic UFT.

dynamics variability in the generated dataset. It is worth noting that determining the number of specimens and test repetitions required to generate a robust data set remains a topic for future research, as the variability in material properties and specimen geometry poses

significant challenges. Also, the variation in the elastic modulus E has not been considered in this study. Instead, it is assumed that variations in E are directly reflected in the variation of measured strain. However, future studies should refine the analysis by considering different sources of uncertainty.

Despite setting a deterministic target tip displacement in the controller, deviations in maximum absolute tip displacement are observed due to noise and experimental conditions, leading to a probabilistic distribution of tip displacement. Similarly, measured strain values for each test repetition showed slight variations in their means and standard deviations due to experimental conditions and DIC correlation residuals as discussed in Section 4.1. Consequently, each displacement setting resulted in slightly different strain values, emphasising the need for a probabilistic distribution for measured strain. The measured data, represented by black dots in Fig. 8b, is used to fit Gaussian distributions to both strain and tip displacement data, representing the 50 data sets at each stress level. The measured data is used to fit Gaussian distributions to both strain and tip displacement data representative of the 50 data sets at each stress level. This allows one to generate further data for statistical analysis. These may be called hidden hierarchies of uncertainties. The fitted distributions are used to carry out a Monte Carlo simulation to generate further data points for tip displacement and strain. Afterwards, the generated data is used within a Bayesian framework explained in Section 3 to fit a probabilistic model to the data. For this purpose, the model in Eq. (9) is used due to the linear nature of the relationship.

$$\epsilon_i = \theta U_i + \epsilon_i \quad (\epsilon_i \sim \mathcal{N}(0, \sigma^2)) \quad (9)$$

where ϵ and U are measured strain and tip displacement. Here, θ is the model parameters and ϵ is the prediction error, which is characterised by a zero mean Gaussian distribution with standard deviation σ . In the hierarchical model configuration, θ is modelled as statistically independent, assumed to follow a normal distribution with mean μ_θ and covariance Σ_θ .

Fig. 8a shows the resulting posterior distribution of parameters, as computed based on Eq. (8), and their correlation analysis. The diagonal subplots show the histograms of the posterior samples, and the off-diagonal subplots indicate the contour plots of the joint posterior distributions of the parameters. The contour plots for the pairs, including the noise standard deviation, indicate that there is no strong correlation between σ , and the model parameters. This means that the noise cannot be modelled with the simple linear model, and its source is the variability discussed in Fig. 7. Besides, the mean value $\sigma = 50$ means that there is $3 \times 50 \mu$ strain variability that could be expected for measured strains under experimental conditions. By employing the estimated parameters, the probabilistic prediction of strain based on target tip displacement can be obtained. Fig. 8b depicts the mean prediction obtained along with uncertainty bounds (i.e., confidence intervals 90 and 99%). It can be observed that all experimental points used in the Bayesian inference are well contained within the uncertainty bounds. This prediction was compared to the analytical equation proposed to predict the strain from tip displacement in [16], which shows a good agreement.

5. Stress-life curves

When the machine is calibrated, one can record stress-life data and build a statistical model to predict the number of cycles to failure based on the applied stress level (see Fig. 7). It has been demonstrated in [13] that the HB method is outperforming the conventional probabilistic methods [31,32] in quantifying the uncertainties observed in stress-life predictive curves, especially when a sparse dataset is available. One of the key conclusions from [13] is that using only a few test specimens, such as three per stress level, the HB method achieves the same accuracy as conventional methods. Therefore, the HB method is

Table 3
Stress levels for testing with UFT.

Target tip displacement (μm)	Strain (μ)	Stress (MPa)
12	1475	295
13	1596.65	319
14	1719.45	344
15	1840	368

used in this work to quantify the uncertainty in stress-life prediction curves.

Here, four stress levels are considered, and the elastic modulus is assumed to be $E = 200$ GPa. The strain, stress, and corresponding tip displacement for the 4 stress levels are reported in Table 3. The test was conducted with three different test specimens for each stress level, with one specimen in each stress level kept for validating the accuracy of probabilistic life prediction. The analysis is repeated by randomly varying the validation data among the experimentally available specimens. The best model describing the data is shown in Fig. 9a along with experimental stress-life data. It can be observed that the variation of the number of cycles to failure is higher for low stresses.

In this step, the stress data is initially augmented based on the probabilistic inference from the model in Eq. (9). The blue squares in Fig. 9b show the augmented data points. The obtained number of cycles to failure is affected by the uncertainty in the applied load under experimental conditions and the material's microstructural variability, which is accounted for by testing multiple specimens under different loading conditions. Consequently, the experimental variability in fatigue life is a function of both load uncertainty and material variability, which cannot necessarily be distinguished. The data for the number of cycles to failure and the probabilistic distribution of stress calculated from the model in Eq. (9) is used to generate an augmented stress-life dataset. This is done via fitting a Bayesian linear model between stress and life and using them to generate further data points [13], which are shown with yellow dots in Fig. 9b. This dataset is used within the HB method explained in Section 3 to generate a probabilistic model to quantify uncertainties in the form of posterior probability distributions, which enables the user to make predictions with a sense of confidence. The probabilistic model used to fit the VHCF data points is presented in Eq. (10).

$$\ln(N_i) = \alpha S_i + \beta + \epsilon_i \quad (\epsilon_i \sim \mathcal{N}(0, \sigma^2)) \quad (10)$$

where N and S are the experimental number of cycles to failure and stress level, respectively. Here, α and β are the model parameters, and ϵ is the prediction error, which is characterised by a zero mean Gaussian distribution with standard deviation σ . The statistical information about the model parameters is reported in Table 4 in terms of mean and standard deviation. By employing the results in Table 4 and Eq. (10), the stress-life curves are generated using the HB method. From Fig. 10a, it can be seen that this method provides a mean prediction as well as confidence intervals of prediction for life in terms of the number of cycles to failure. Both 90% and 99% confidence intervals are plotted. The plot also includes the validation data points within the 90% confidence interval that demonstrate the accuracy of the probabilistic linear model in predicting life in the VHCF region. The trend indicates that assuming infinite life for EN8 metal might be conservative.

Furthermore, Akram et al. [27] reported data from a high-cycle fatigue test conducted using a rotating bending machine with a working frequency of 63 Hz for EN8 steel. The data points from the high-cycle to the VHCF region are combined here. Eq. (11) is used to produce a probabilistic model for both regions using the HB method described in Section 3.

$$\ln(N_i) = ((S_i - c)/\alpha)^{1/\beta} + \epsilon_i \quad (\epsilon_i \sim \mathcal{N}(0, \sigma^2)) \quad (11)$$

where α , β and c are the model parameters. The mean and standard deviation for the model parameters are reported in Table 4 along with

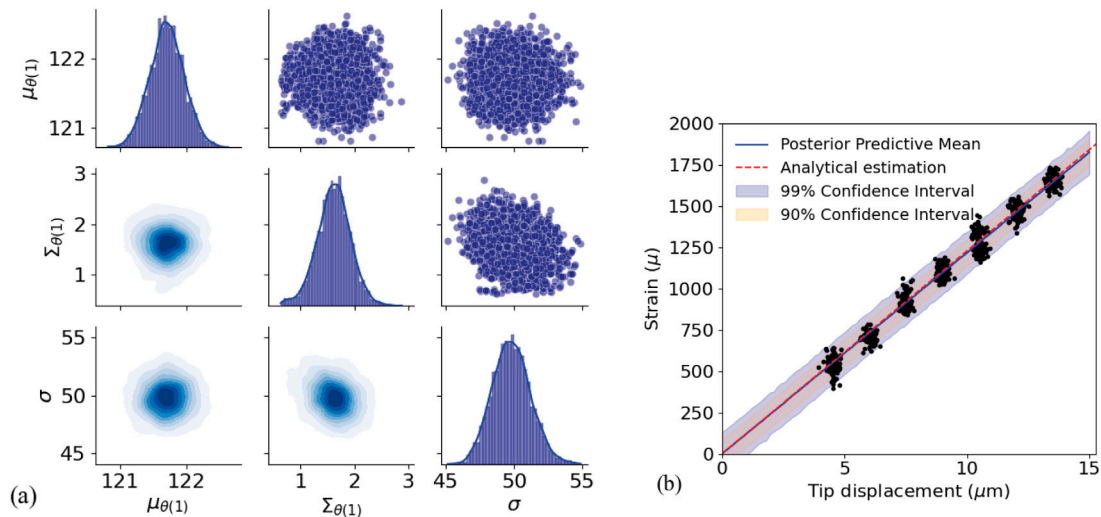


Fig. 8. Uncertainty quantification and propagation (a) posterior distribution and correlation analysis of the parameters; (b) probabilistic prediction of strain–displacement relationship (black dots present the measured data).

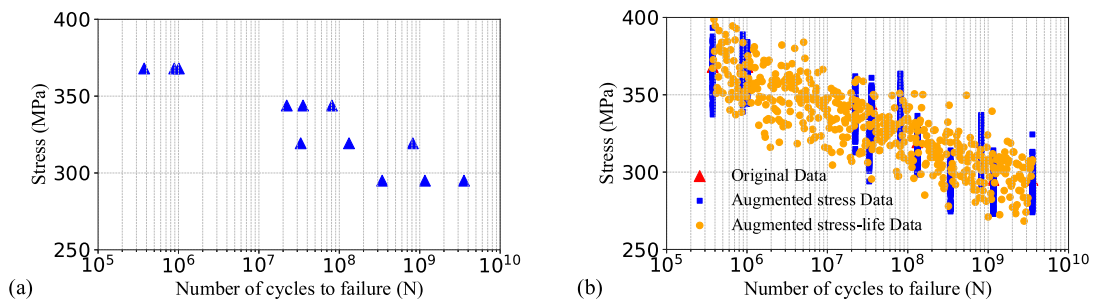


Fig. 9. Stress-life data (a) raw experimental data; (b) augmented stress and stress-life data.

Table 4
Second-moment statistical information for S-N curve models.

θ_i	VHCF data		Full S-N data	
	$E[\theta_i]$	$SD[\theta_i]$	$E[\theta_i]$	$SD[\theta_i]$
α	-0.086	0.0014	53777634.8	10.06
β	46.08	0.46	-5.27	0.02
c	-	-	304.02	4.9
σ	1.38	0.03	19.3	2.18

θ_i - Estimate value of the i th parameter.
 $E[\theta_{(i)}]$ - Expected value of parameter estimated by sampling.
 $SD[\theta_{(i)}]$ - Standard deviation of parameter estimated by sampling.

the standard deviation of the prediction residual. The first observation is that when fitting a single model to data from all regions of the stress-life curve, the prediction residual increases compared to the model fitted only to the VHCF region. This suggests that using different forms for different regions of the stress-life curve may lead to better accuracy in the prediction. This is a topic of current research.

To display the predicting properties of the HB method, the samples drawn from the posterior distribution of hyperparameters are used to construct the probabilistic stress-life curves, as depicted in Fig. 10b. It can be seen that the data points all exist within the uncertainty bounds shown by the confidence interval, and the mean accurately predicts the life cycles. Again, it can be seen that fitting all data at once may result in over-conservative trends and uncertainty bounds as compared to using different equations to describe the behaviour of different regions of the stress-life curve. Nonetheless, combining the data from low- and high-frequency tests depends not only on frequency but also on the

specimen size and different testing environments. Furthermore, there is no run-out sample within the specimens used in this study, and no assumption can be made about the fatigue limit within the stress-life range used in this study. We avoid drawing a general conclusion here, as investigating these effects is the subject of future research.

6. Discussion on variability

This section discusses the possible sources of variability observed in the calibration curve (Fig. 8) and the stress-life curves (Fig. 10) in this study. In general, the source of variability could be the testing procedure and material variability. Testing procedure variability includes loading, testing equipment, measurement system, frequency effects, and environmental effects such as temperature and humidity. Material variability sources include specimen size effect, microstructural features, surface treatment, etc. This paper aimed at quantifying variabilities sourced from the UFT testing equipment operation and the measurement systems via generating Fig. 8. In addition, those variabilities are transferred to the stress-life prediction by testing multiple specimens, which results in considering microstructural feature variability in particular.

Regarding material variability, a general discussion based on the probabilistic stress-life curves for EN8 steel highlights the high uncertainty in life estimation for a specific stress level in the VHCF region. For example, it varies between 2×10^5 and 10^8 with a 90% confidence interval for 350 MPa in Fig. 10a. This raises the question of whether the information about lifetime from UFT is useful and trustworthy. The trend analysis in Fig. 10a shows that even though the uncertainty is high, there is a finite life for low stresses. To understand

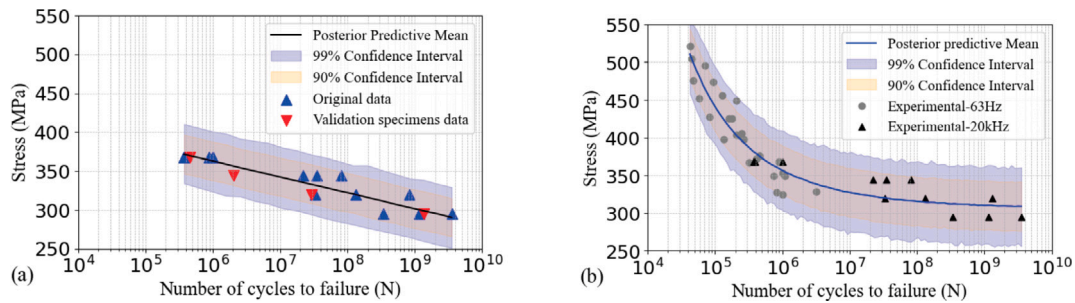


Fig. 10. Stress-life curve and prediction confidence interval for the EN8 steel (a) VHCF data; (b) all range stress-life dataset. Source: Experimental 63 Hz data has been reproduced from [27].

this high uncertainty, an important explanation in the Japanese WES 1112 standard [17] is that UFT is suitable for high-strength steels with a tensile strength of over 1200 MPa. Whereas EN8 carbon steel is a ferritic, medium-strength steel with a body-centered cubic (BCC) slip system, and it has been reported that for ferritic materials with BCC slip systems, the cyclic frequency effect may dominate [17,33,34]. The testing frequency or strain rate effect on a similar steel, such as C45E, indicates that a higher testing frequency results in a higher lifetime [35,36]. This could be treated using methods for strain rate dependent correction [37], however, it is outside of the scope of this study. Also, the dispersion could be higher for ferritic steel due to increased heating at very high frequencies, which necessitates more frequent pulse/pause cycles during testing. Additionally, at very high cycle numbers (beyond 10^8), the uncertainty in the location of inclusions for crack initiation along slip bands at the surface leads to significantly greater variability [35], as shown in Fig. 10b.

Lage et al. [16] observed that environmental factors (e.g., temperature) have a significantly greater influence than frequency when comparing results with conventional fatigue tests for EN8 steel. In high-strength steels with higher carbon content, fatigue cracks in the high-cycle fatigue (HCF) region typically initiate at the surface. Conversely, during ultrasonic fatigue testing in the very high cycle fatigue (VHCF) regime, crack initiation often occurs internally around inclusions, leading to the elimination of a distinct fatigue limit. Although EN8 steel is not classified as high-strength steel, fatigue crack initiation in the VHCF regime has been observed to occur internally [16], forming a characteristic ‘fish-eye’ fracture pattern. Treating the source of high dispersion in the VHCF region for medium-strength EN8 steel still remains an open research topic that falls outside of the scope of this paper. For this purpose, a detailed fractography of the fracture surface should be considered in future works to identify the source of fatigue cracks, etc.

7. Summary

Even though ultrasonic fatigue tests operating at 20 kHz can straightforwardly reach a very high number of cyclic loads (beyond 10^7) in an accelerated fashion, the high dispersion of stress-life data could indicate uncertainties involved in the calibration and operation of the machine. The main sources of uncertainties are microstructural variabilities during the material processes and operational variabilities during the UFT. This work considers both material uncertainties by running the test for a couple of specimens with the same stress level and operational uncertainties via a statistical calibration process.

The ultimate controlling parameter of stress in a UFT specimen is the tip displacement. Therefore, the variability of displacement measurement and the induced highest linear stress are accounted for during the calibration phase of the UFT machine using multiple datasets. This led to a probabilistic calibration curve, i.e., tip displacement vs. stress. The probabilistic calibration curve and the number of cycles to failure data from multiple specimens are used to build another probabilistic

relationship that describes the S-N curve. This is all taken forward using the HB method that eventually provides the confidence interval for the material lifetime estimation. These calculated confidence intervals include the calibration and testing uncertainties. The results for a medium-strength metal with ferritic content indicate that there is a high uncertainty in the estimated lifetime. However, the trend of the stress-life curve shows a finite life in the VHCF regime.

This research does not aim to generalise the conclusions due to the limited number of datasets and materials used; however, it proposes a technique to understand and reflect on the experimental uncertainties involved in the UFT. There are other factors affecting the experiment that should be included in future studies. These include the temperature control strategy, sample size effect, the rising time of excitation to the target steady-state level, and cycles due to decaying from stops for the cooling interventions. Future works could investigate a detailed microstructural analysis of EN8 steel and its relationship with the current lifetime observations, while also quantifying the possible contribution to scatter caused by different factors.

CRediT authorship contribution statement

Sina Safari: Writing – original draft, Visualization, Validation, Software, Methodology, Formal analysis, Data curation, Conceptualization. **Diogo Montalvão:** Writing – review & editing, Supervision, Resources, Methodology, Investigation, Funding acquisition, Conceptualization. **Pedro R. da Costa:** Writing – review & editing, Resources, Investigation. **Luís Reis:** Writing – review & editing, Supervision, Resources, Investigation, Funding acquisition. **Manuel Freitas:** Writing – review & editing, Supervision, Resources, Investigation.

Code availability

A demo source code developed for this work is available on GitHub at <https://github.com/sinaplatform/Hierarchical-Bayesian-demo>

Declaration of competing interest

The authors declare that they have no known competing financial interests or personal relationships that could have appeared to influence the work reported in this paper.

Acknowledgements

The authors acknowledge Research England (United Kingdom), through the ADDISONIC’s Bournemouth University Strategic Investment Area. Also, the authors acknowledge Fundação para a Ciência e a Tecnologia (FCT) for its financial support via the projects LAETA Base Funding, UK (DOI: 10.54499/UIDB/50022/2020) and LAETA Programatic Funding, UK (DOI: 10.54499/UIDP/50022/2020).

Appendix A. Supplementary data

Supplementary material related to this article can be found online at <https://doi.org/10.1016/j.ijfatigue.2025.109028>.

Data availability

Data will be made available on request.

References

- [1] Stanzl S, Tschegg E, Mayer H. Lifetime measurements for random loading in the very high cycle fatigue range. *Int J Fatigue* 1986;8(4):195–200.
- [2] Stanzl S. Fatigue testing at ultrasonic frequencies. *J Soc Environ Eng* 1986;25:11–6.
- [3] Bathias C, Jingang N. Determination of fatigue limit between 10⁵ and 10⁹ cycles using an ultrasonic fatigue device. In: *Advances in fatigue lifetime predictive techniques: second volume*. ASTM International; 1993.
- [4] Hong Y, Sun C. The nature and the mechanism of crack initiation and early growth for very-high-cycle fatigue of metallic materials—an overview. *Theor Appl Fract Mech* 2017;92:331–50.
- [5] Mason WP, Baerwald H. Piezoelectric crystals and their applications to ultrasonics. *Phys Today* 1951;4(5):23–4.
- [6] Stanzl S, Hollanek W, Tschegg E. Fatigue and fracture under variable-amplitude loading at ultrasonic frequency. In: *Fracture* 84. Elsevier; 1984, p. 3645–51.
- [7] Costa P, Nwawe R, Soares H, Reis L, Freitas M, Chen Y, Montalvão D. Review of multiaxial testing for very high cycle fatigue: From ‘conventional’ to ultrasonic machines. *Mach* 2020;8(2):25.
- [8] Tridello A, Niutta CB, Haghshenas M, Berto F, Paolino DS. 1.09 - very high cycle fatigue (VHCF) of materials: An overview. In: Silberschmidt V, editor. *Comprehensive mechanics of materials (first edition)*. First Edition. Oxford: Elsevier; 2024, p. 192–220. <http://dx.doi.org/10.1016/B978-0-323-90646-3.00007-1>, URL <https://www.sciencedirect.com/science/article/pii/B9780323906463000071>.
- [9] Tahmasbi K, Alharthi F, Webster G, Haghshenas M. Dynamic frequency-dependent fatigue damage in metals: A state-of-the-art review. *Forces Mech* 2023;10:100167.
- [10] Furuya Y, Shimamura Y, Takanashi M, Ogawa T. Standardization of an ultrasonic fatigue testing method in Japan. *Fatigue Fract Eng Mater Struct* 2022;45(8):2415–20.
- [11] Montalvão D, Blaskovics A, Costa P, Reis L, Freitas M. Numerical analysis of VHCF cruciform test specimens with non-unitary biaxiality ratios. *Int J Comput Methods Exp Meas* 2019;7(4):327–39.
- [12] da Costa PR, Rahaeifard M, Montalvão D, Reis L, Freitas M. A new method for ultrasonic fatigue component frequency modulation: From ultrasonic horn to uniaxial and multiaxial specimens. *Int J Fatigue* 2023;176:107887.
- [13] Chen J, Liu S, Zhang W, Liu Y. Uncertainty quantification of fatigue SN curves with sparse data using hierarchical Bayesian data augmentation. *Int J Fatigue* 2020;134:105511.
- [14] Terrazas VF, Sedehi O, Papadimitriou C, Katafygiotis LS. A Bayesian framework for calibration of multiaxial fatigue curves. *Int J Fatigue* 2022;163:107105.
- [15] Liu X-W, Lu D-G. Survival analysis of fatigue data: Application of generalized linear models and hierarchical Bayesian model. *Int J Fatigue* 2018;117:39–46.
- [16] Lage Y, Ribeiro A, Montalvão D, Reis L, Freitas M. Automation in strain and temperature control on VHCF with an ultrasonic testing facility. *Appl Autom Technol Fatigue Fract Test Anal (ASTM Spec Tech Publication)* 2014;80–100.
- [17] *Method for ultrasonic fatigue testing in metallic material*. Technical Report WES 1112, Tokyo, Japan: The Japan Welding Engineering Society; 2022.
- [18] instruments N. Istra4D V4.11 release note. 2024, URL <https://www.dantecdyna.com/wp-content/uploads/2024/10/DDS-DIC-ISTRA4D-RELV411-EN-V1-1.pdf> (Accessed 26 March 2025).
- [19] Lage Y, Freitas M, Reis L, Ribeiro A, Montalvão D. Instrumentation of ultrasonic high-frequency machine to estimate applied stress in middle section of specimen. In: *Procs of 15th international conference on experimental mechanics*. 2012.
- [20] Hoffman MD, Gelman A, et al. The no-u-turn sampler: adaptively setting path lengths in Hamiltonian Monte Carlo. *J Mach Learn Res* 2014;15(1):1593–623.
- [21] Vanik MW, Beck JL, Au S-K. Bayesian probabilistic approach to structural health monitoring. *J Eng Mech* 2000;126(7):738–45.
- [22] Wu S, Angelikopoulos P, Beck JL, Koumoutsakos P. Hierarchical stochastic model in Bayesian inference for engineering applications: Theoretical implications and efficient approximation. *ASCE- ASME J Risk Uncertain Eng Syst Part B: Mech Eng* 2019;5(1):011006.
- [23] Hastings WK. Monte Carlo sampling methods using Markov chains and their applications. 1970.
- [24] Geman S, Geman D. Stochastic relaxation, gibbs distributions, and the Bayesian restoration of images. *IEEE Trans Pattern Anal Mach Intell* 1984;6(6):721–41.
- [25] Abril-Pla O, Andreani V, Carroll C, Dong L, Fannesbeck CJ, Kochurov M, Kumar R, Lao J, Luhmann CC, Martin OA, et al. Pymc: a modern, and comprehensive probabilistic programming framework in python. *PeerJ Comput Sci* 2023;9:e1516.
- [26] Costa P, Vieira M, Reis L, Ribeiro A, de Freitas M. New specimen and horn design for combined tension and torsion ultrasonic fatigue testing in the very high cycle fatigue regime. *Int J Fatigue* 2017;103:248–57.
- [27] Akram S, Babutskyi A, Chrysanthou A, Montalvão D, Pizurova N. Effect of alternating magnetic field on the fatigue behaviour of EN8 steel and 2014-T6 aluminium alloy. *Metals* 2019;9(9):984.
- [28] Jones EM, Iadicola MA, et al. A good practices guide for digital image correlation. *Int Digit Image Correl Soc* 2018;10:1–110.
- [29] Londoño JM, Neild SA, Cooper JE. Identification of backbone curves of nonlinear systems from resonance decay responses. *J Sound Vib* 2015;348:224–38.
- [30] Safari S, Monsalve JL. Data-driven structural identification of nonlinear assemblies: Structures with bolted joints. *Mech Syst Signal Process* 2023;195:110296.
- [31] Xie L, Liu J, Wu N, Qian W. Backwards statistical inference method for P–s–n curve fitting with small-sample experiment data. *Int J Fatigue* 2014;63:62–7.
- [32] Collins JA. *Failure of materials in mechanical design: analysis, prediction, prevention*. John Wiley & Sons; 1993.
- [33] Mughrabi H. Cyclic strain rate effects in fatigued face-centred and body-centred cubic metals. *Phil Mag* 2013;93(28–30):3821–34.
- [34] Mughrabi H. Microstructural mechanisms of cyclic deformation, fatigue crack initiation and early crack growth. *Philos Trans R Soc A: Math Phys Eng Sci* 2015;373(2038):20140132.
- [35] Torabian N, Favier V, Dirrenberger J, Adamski F, Ziaei-Rad S, Ranc N. Correlation of the high and very high cycle fatigue response of ferrite based steels with strain rate-temperature conditions. *Acta Mater* 2017;134:40–52.
- [36] Bach J, Möller J, Göken M, Bitzek E, Höppel H. On the transition from plastic deformation to crack initiation in the high-and very high-cycle fatigue regimes in plain carbon steels. *Int J Fatigue* 2016;93:281–91.
- [37] Geilen MB, Klein M, Oechsner M, Kaffenberger M, Störzel K, Melz T. A method for the strain rate dependent correction for control type of fatigue tests. *Int J Fatigue* 2020;138:105726.